

Plasma-Enhanced Molecular Layer Deposition of Phosphane–Ene Polymer Films

Justin T. Lomax, Eden Goodwin, Peter G. Gordon, Christine McGuinness, Floryan De Campo, Seán T. Barry,* and Paul J. Ragogna*



Cite This: *Chem. Mater.* 2023, 35, 1579–1585



Read Online

ACCESS |



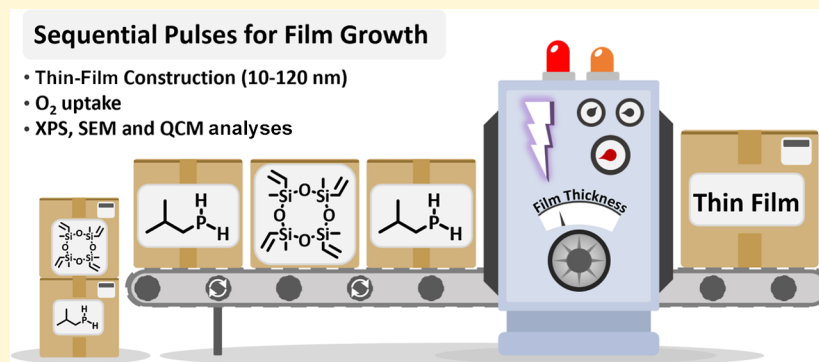
Metrics & More



Article Recommendations



Supporting Information



ABSTRACT: A vapor-phase molecular layer deposition (MLD) process generating phosphorus-rich phosphane–ene polymer networks was adapted from known solution-phase methods and successfully used in a commercial atomic layer deposition tool. By using plasma-enhanced MLD on Si/SiO₂ and Al₂O₃ substrates, film deposition was carried out with a commercially available primary phosphine, *i*BuPH₂, paired with a known volatile cyclic siloxane precursor, tetramethyltetravinylcyclotetrasiloxane (D₄^{Vinyl}). The deposition process used radicals generated by an Ar plasma source to facilitate P–H addition to vinyl functionalities on D₄^{Vinyl} which yielded a growth per cycle of 0.6–2.0 Å, generating 10–120 nm films as determined by atomic force microscopy and scanning electron microscopy measurements. Characterization of the films were carried out using X-ray photoelectron spectroscopy, and oxygen scavenging capabilities were studied using a quartz crystal microbalance, showing an uptake of oxygen by a 12 nm depth of a freshly deposited polymer film.

INTRODUCTION

Molecular layer deposition (MLD) is a type of atomic layer deposition (ALD), where organic thin films are deposited from the vapor phase through sequential, self-limiting reactions, generating thin films with high tunability, uniformity, and conformality.¹ MLD as a technique was first discovered by Yoshimura et al. in 1991 to prepare polyimides through a diamine (2,4-diaminonitrobenzene or 4,4'-diaminodiphenyl ether) and pyrometallic dianhydride,² and since its introduction many compounds have been employed as precursors to generate thin films of materials with thicknesses on the nanometer scale. Examples include amides, ureas, thioureas, azomethines, and ethylene terephthalates.^{3–6} MLD is still in its infancy as compared to ALD; therefore, relatively few elements other than C, N, O, and S have been incorporated in these thin films, leaving many paths open for investigation.¹

Emerging technologies such as high-capacity batteries and flexible microelectronic devices can leverage MLD films to solve problems that are preventing their widespread use and commercialization. Through the formation of ultrathin,

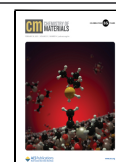
resilient, and flexible polymer networks, MLD will be a primary driver going forward. The Ragogna group has developed a method to synthesize robust phosphorus polymer networks from the bulk phase using a thermal- or photo-initiator that shows excellent surface adhesion, barrier properties to O₂, optical transparency in the visible spectrum, and thermal stability up to 400 °C.^{7–9} Phosphane–ene polymer networks propagate by the formation of a phosphinyl radical, which adds to a vinyl cross-linking agent to propagate the polymer growth.^{7,10–12}

These phosphane–ene polymer networks are a class of materials that can be easily tuned to bind transition metals and scavenge oxygen; it is this second characteristic that holds

Received: October 6, 2022

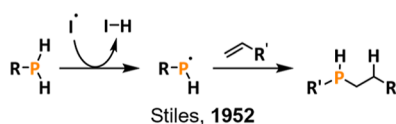
Revised: December 12, 2022

Published: January 4, 2023



promise for these networks as packaging and protecting layers for flexible electronics. Phosphane–ene polymer networks are typically fabricated by reacting a primary phosphine (i.e., PH_3 , CyPH_2 , or $i\text{BuPH}_2$) and a multifunctional olefin crosslinking agent. By changing the composition of the monomer, the thermal, mechanical, and chemical properties of the resulting polymer can easily be modified.^{7,8,13} Since some typical vinyl crosslinkers showed reasonable volatility, it seemed viable to transfer this solution-phase polymerization chemistry to an MLD process (Figure 1). In this context, we report successful

Radical-mediated hydrophosphination



Phosphane-ene polymer networks

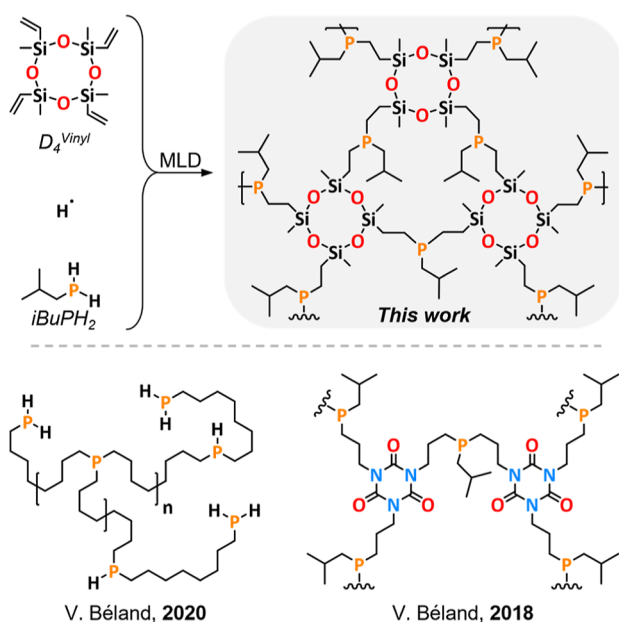


Figure 1. Generic radical-mediated hydrophosphination of an alkene and phosphane–ene polymer networks.

MLD of a phosphane–ene polymer network, including careful thermal characterization of the deposition precursors isobutyl phosphine ($i\text{BuPH}_2$) and the vinyl crosslinker 2,4,6,8-tetramethyl-2,4,6,8-tetravinyl-cyclotetrasiloxane ($\text{D}_4^{\text{Vinyl}}$). To our knowledge, this is the first documentation of radical-mediated phosphine chemistry used in a MLD process. These networks were tested for their reactivity with oxygen using a quartz crystal microbalance (QCM) to monitor the mass gain of the deposited films in an oxygen-rich atmosphere.

RESULTS AND DISCUSSION

The volatility of $\text{D}_4^{\text{Vinyl}}$ and $i\text{BuPH}_2$ were measured by thermogravimetric analysis (TGA) to determine the temperature of volatilization (T_V) and assess their viability as precursors. T_V is defined as a temperature where the compound gives 1 Torr of vapor pressure. This definition arises from the expectation of what comprises a “good” vapor pressure from an industrial perspective: 1 Torr of vapor pressure supplies a significant flux of precursor in most

industrial tools and is within the operating pressure of most ALD tools.^{14–17}

$\text{D}_4^{\text{Vinyl}}$ exhibited a T_V of 52 °C with zero residual mass (Figure 2). The lack of residual mass demonstrates that there is

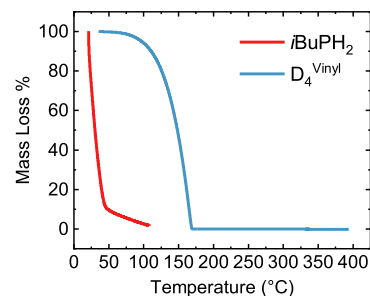


Figure 2. Thermograms of $i\text{BuPH}_2$ and $\text{D}_4^{\text{Vinyl}}$ showing percent change in sample mass under consistent heating at 10 °C/min.

no decomposition during evaporation and along with the low T_V indicated an ideal vinyl crosslinker MLD precursor. The phosphine precursor $i\text{BuPH}_2$ was extremely volatile, as a result its T_V could not be accurately established. $i\text{BuPH}_2$ volatilized at room temperature too quickly for a meaningful TGA trace to be obtained with respect to volatilization. Nevertheless, the TGA trace shows no residual mass, indicating that $i\text{BuPH}_2$ is also a promising MLD precursor. During on-tool process development, it was established that significant cooling (to 7 °C) is required to deliver a reasonable flux of $i\text{BuPH}_2$.

The decomposition temperature as measured by differential scanning calorimetry (DSC) in a sealed pan was also measured for vapor precursors to provide a “thermal range” between the volatilization melting point (−44 °C) and boiling point (110 °C), which might be due to the decomposition involving the pan wall. The decomposition of $\text{D}_4^{\text{Vinyl}}$ was well outside the operating range of the precursor for deposition (Figure S1). A DSC trace for $i\text{BuPH}_2$ could not be and decomposition. $\text{D}_4^{\text{Vinyl}}$ showed an endotherm at 205 °C which does not correspond to the collected compound due to the extremely high volatility of the compound at low temperatures, which caused the sealed measurement pans to rupture before any relevant data could be collected. These thermal characteristics suggested that the MLD should be a low-temperature process.

No film growth was observed with thermal MLD conditions using only $i\text{BuPH}_2$ and $\text{D}_4^{\text{Vinyl}}$ at 200 °C. This was expected since the solution polymerization method requires a radical species for polymerization to be initiated.⁷

After significant optimization of pulse sequencing, testing plasma pulses at various points in the process, a successful MLD process was developed using $i\text{BuPH}_2$, $\text{D}_4^{\text{Vinyl}}$, and an argon plasma [(Ar*) (5.0 Ar at 2800 W)], with the plasma serving as the radical mediator. A typical deposition began by heating the deposition chamber to 200 °C, followed by 10 pulses of hydrogen plasma (5% H_2/Ar) to remove any surface contamination and to ensure that each of the depositions began with a standard, clean surface. The $i\text{BuPH}_2$ bubbler was cooled with a chiller to 7 °C, and the $\text{D}_4^{\text{Vinyl}}$ precursor was held at 75 °C. The pulse program after the plasma cleans consisted of a 0.1 s pulse of $i\text{BuPH}_2$, followed by a 10 s purge (N_2); a 0.1 s pulse of $\text{D}_4^{\text{Vinyl}}$, followed by a second 10 s purge; and a 10 s pulse of Ar plasma at 2800 W with no purge. These three pulses constituted a single cycle, and typically 300 cycles were used to generate the films reported here. Changes in growth

behavior, film morphology, and degree of crosslinking as a result of deposition temperature are currently being investigated for subsequent publication.

We speculate that the *i*BuPH₂ precursor reacts with Ar* by abstraction of a hydrogen from *i*BuPH₂ to generate a phosphinyl radical to add to a surface vinyl functional group (Figure 3a). This leaves a second P–H bond remaining on the

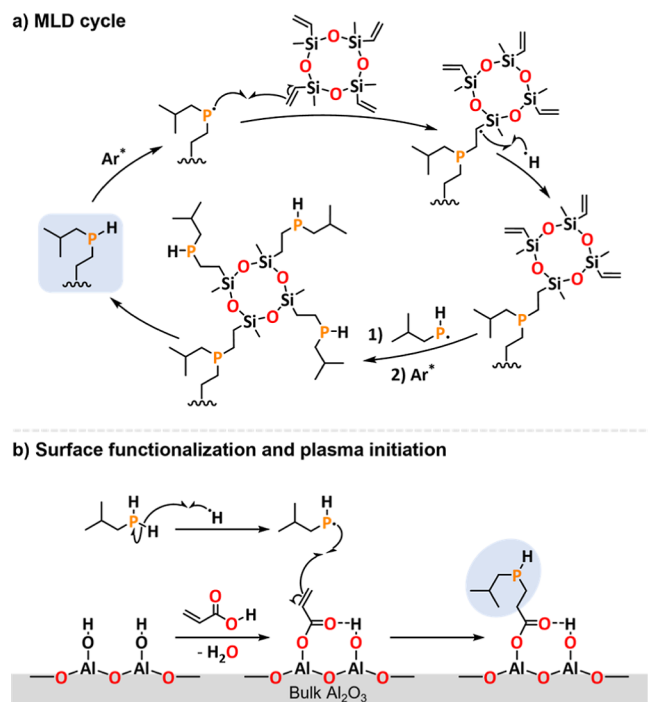


Figure 3. Proposed scheme of phosphane–ene film growth by MLD with *i*BuPH₂ and D₄^{Vinyl} mediated by an Ar plasma (Ar*) for radical initiation and propagation of precursors.

surface, and subsequent radical P* formation will then add to the vinyl crosslinker D₄^{Vinyl} when it is introduced into the chamber, propagating film growth.

In an attempt to promote substrate-enhanced growth during the MLD process, Al₂O₃ substrates were primed with a variety of carboxylic acids by dip-coating: acrylic acid (AA), pentanoic acid (PA), and undecylenic acid (UA) were each assessed as surface primers.¹⁸ These primers were chosen to probe the effects of varying the alkyl chain length of the vinyl functional group on phosphine nucleation. It is expected that by providing initial surface-bound vinyl groups, the surface reactivity of the *i*BuPH* radical would be enhanced and promote the film growth (Figure 3b).

The saturation curve for the D₄^{Vinyl} precursor with Ar* in the absence of a surface primer group (Figure 4) suggests saturated growth but with a higher than usual variability than expected for MLD processes. There may be competing reversible and irreversible surface nucleation that is causing this variability, and further surface mechanistic studies will be required to determine how chemisorption and growth proceed in this process. For 600-cycle long pulse regimes with 0.1 s *i*BuPH₂ pulses, we observe significant (>3 g) mass loss from the bubbler. The minimum pulse duration for this ALD tool is 0.1 s, resulting in the same growth per cycle (GPC) at every measured point for *i*BuPH₂.

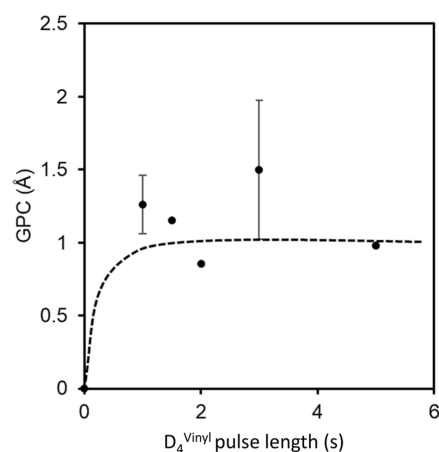


Figure 4. Saturation curve showing film GPC as a function of D₄^{Vinyl} pulse length where Ar* and the *i*BuPH₂ pulse lengths are held at 0.1 s. Plateauing of GPC at increasing pulse durations indicates self-limiting behavior.

Phosphane–ene films were analyzed through atomic force microscopy (AFM) to determine their thickness and surface morphology (Figures S1,ii). Step edges were created using Kapton tape to mask part of the substrate, and postdeposition the tape was removed with tape residue only on the bare Si wafer cleaned with isopropyl alcohol. Similar 300-cycle depositions resulted in an average GPC of 0.7 Å. In addition to the characterization of the film thickness by AFM, focused ion beam scanning electron microscopy (FIB-SEM) images were collected (Figure S1iii). The cross-sectional view of the film was in good agreement with the thickness measured by AFM and showed excellent conformality of the film deposited on SiO₂ with a film thickness of 20 nm after 300 cycles. The resulting films had a root-mean-square roughness of 4.7 Å, close to that measured for the substrate (9.0 Å). As is typical with MLD processes, the films had consistent smooth coverage.^{19,20}

Elemental composition and bonding environments of phosphane–ene films on Al₂O₃ were analyzed using X-ray photoelectron spectroscopy (XPS). Due to the thinness (20 nm) of grown films, accurate elemental composition could not be obtained using techniques with high-penetration depths, such as energy-dispersive X-ray spectroscopy. To estimate the relative inclusion of both precursors (*i*BuPH₂ and D₄^{Vinyl}) in the film, a ratio of Si 2p and P 2p peak areas was calculated from XPS survey scans. Initial deposition trials were attempted with *i*BuPH₂ (0.1 s pulse, 10 s purge) and D₄^{Vinyl} (1 s pulse, 10 s purge) on AA-primed Al₂O₃ (AA-Al₂O₃). These films had 1.2 and 4.4% for Si 2p and P 2p, respectively, giving a ratio of 0.27:1 compared to an ideal ratio of 2:1 Si:P. This lower ratio suggests an incomplete reaction of D₄^{Vinyl}. This deposition was repeated with a precleaned 5% H₂/Ar plasma prior to primer adsorption, which improved the Si/P ratio to 0.44:1. XPS data from a similar run but using a longer D₄^{Vinyl} pulse (10 s) gave a Si/P ratio of 1.44:1, showing that longer D₄^{Vinyl} pulses increases the ratio of Si to P in the film. This observation combined with no observable thickness change at longer D₄^{Vinyl} pulses implies a relationship between the pulse duration and the degree of crosslinking. The lower Si/P ratio could be caused by excess *i*BuPH₂ diffusing through the bulk polymer and reacting with noncrosslinked vinyl groups.

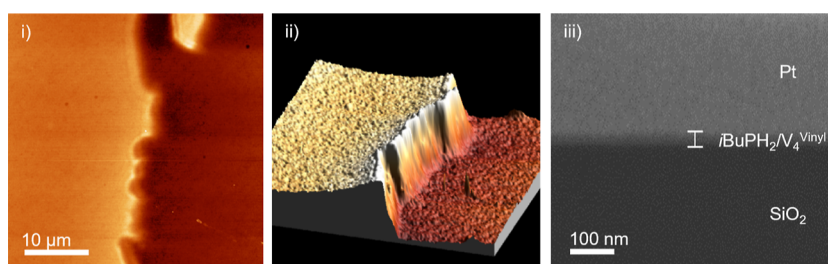


Figure 5. (i) AFM image of a phosphane-ene film with a step edge of 20.9 nm on a Si substrate. (ii) 3D topographical AFM image of the film. (iii) FIB-SEM cross section of the phosphane-ene film with a film thickness of 20 nm (contrast +100%).

Although other primers were used to promote substrate-enhanced growth, all XPS data indicated that, in each case, the priming agents resulted in inferior films when compared to the bare substrates (Table 1). The literature provides a rationale

Table 1. Tabulated XPS Data of P and Si Atomic % from Phosphane-ene MLD runs^a

Substrate	primer	Si/P (at. % ratio)		
		(i)	(ii)	(iii)
Al ₂ O ₃		0.59	0.67	2.19
	AA	0.27	0.44	1.44
	PA	0.28	0.09	1.83
	UA	0.24	0.42	1.49
Au		0.25	0.12	1.92
	AA	0.33	0	1.4
	PA	0.23	1.06	1.54
	UA	0	0	1.13

^aPulse parameters used were (i) *i*BuPH₂ (0.1 s/10 s), D₄^{Vinyl} (1 s/10 s), and Ar[•] (12 s, 2800 W) with no H[•] plasma cleaning, (ii) repeat of (i) with plasma cleaning, and (iii) repeat of (ii) with a 10 s D₄^{Vinyl} pulse. Each run consisted of 300 cycles. The anticipated Si/P ratio of a fully crosslinked film is 2, with error on XPS Si and P measurements of 0.5 at. %.

for the observed film growth on bare Al₂O₃ substrates, where D₄^{Vinyl} can undergo ring opening on the Al₂O₃ surface, thus enabling film growth via the remaining, pendant vinyl

functional groups.^{21,22} In addition to Al₂O₃, Au-coated substrates were probed to evaluate growth on nonoxide surfaces. Lower than anticipated Si/P ratios were observed, particularly for processes with 1s D₄^{Vinyl} pulses. Low to no growth was observed on plasma-cleaned Au surfaces, suggesting that nonoxide surfaces are unable to initiate growth. For a plasma-cleaned Au surface, an increase in D₄^{Vinyl} pulse duration to 10 s resulted in a Si/P ratio that better aligns with values predicted for a fully cross-linked polymer network (2:1, Si/P). This observation implies a loss of selectivity when D₄^{Vinyl} has time to nucleate on the surface.

From XPS data, P 2p, Si 2p, and C 1s core-level spectra with peak-fitting were all modeled with Gaussian-Lorentzian functions and a Shirley background subtraction (Figure 6a). The P 2p spectra was deconvoluted into P(V) and P(III) states. For P(V), there was a signal for fully oxygen-bonded as well as oxygen- and alkyl-bonded phosphorus at 134.1 and 133.5 eV, respectively. This film also showed contributions from a fully alkyl-bonded P(III) center at 130.7 eV. The abundance of P-O centers in the P 2p spectrum is attributed to surface oxidation from the ex situ XPS analysis, while PR₃ species for the film is a manifestation of P(III) bonding environments within the film that have not been oxidized as diffusion of O₂ had not reached the full depth of the film. The Si 2p spectrum displays one assignment of siloxane from the D₄^{Vinyl} at a binding energy (BE) of 102.6 eV.²³ Deconvolution of the C 1s spectra of the film on the Al₂O₃ substrate contains bonding configurations of C-Si-C and C-P=O with BEs of

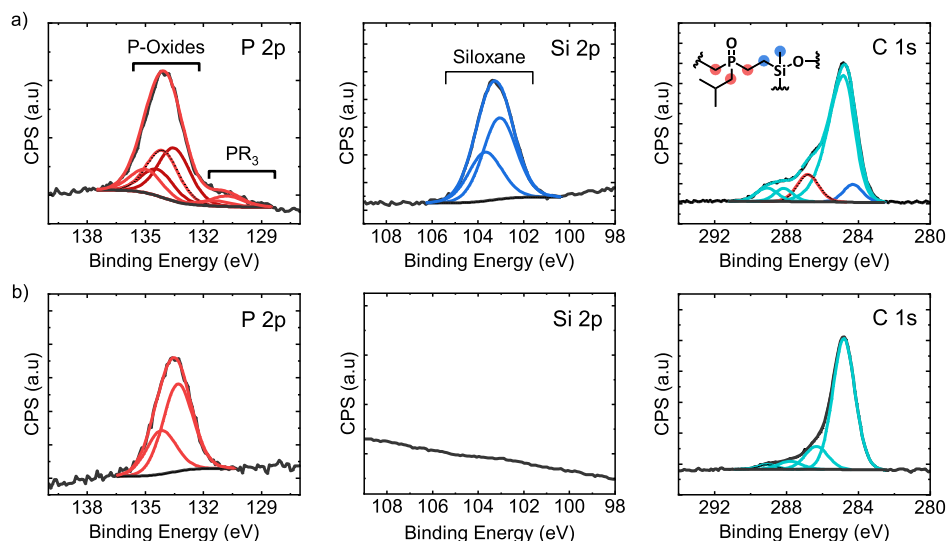


Figure 6. High-resolution P 2p, Si 2p, and C 1s XPS spectra of films on (a) Al₂O₃, at. % (P 2p—3.6%, Si 2p—3.8%, and C 1s—22.2%) and (b) Au, at. % (P 2p—8.7%, Si 2p—0%, and C 1s—30.8%); expected at. % (P 2p—6.3% and Si 2p—12.5%).

284.3 and 286.8 eV, respectively.²⁴ The C 1s spectrum also showed some surface contaminants C–O–C, C=O, and O–C=O with BEs of 286.6, 287.8 and 289.0 eV, respectively, and is attributed to adventitious carbon.^{25,26} Given the inaccuracies that arise from adventitious carbon species, the area of the C–P=O connection in the C 1s is higher than expected but overlaps with C–O–C BEs which is a common impurity.

On the Au substrate, the C 1s window shows a lack of C–Si–C fittings which would be present for the D_4^{Vinyl} precursor. The P 2p XPS windows on Au substrates show the P-oxide content at higher BE (Figure 6b). The negligible amount of Si suggests only residual (and potentially adventitiously oxidized) $i\text{BuPH}_2$ on the Au substrate.

XPS depth profiling of the deposited phosphane–ene film on Al_2O_3 yielded interesting data pertaining to phosphorus oxidation (Figure 7a). When sputtered, the P 2p high-

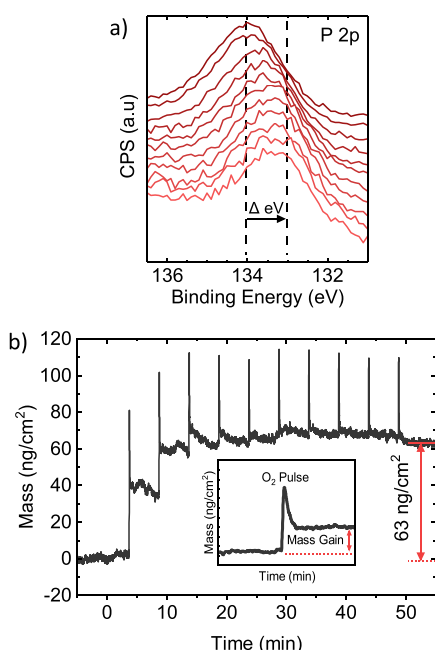


Figure 7. (a) Stacked high-resolution XPS spectra of the sputtered P 2p region, indicating a shift from P^V to P^{III} species ($\Delta = 1.1 \text{ eV}$). (b) QCM trace showing an areal mass density increase due to oxygen uptake of a MLD phosphane–ene film. Inset shows mass gain from a single dry air pulse.

resolution spectra are observed to change to a lower BE closer to the substrate ($\Delta = 1.1 \text{ eV}$). This is likely due to the phosphorus in the polymer reacting with atmospheric oxygen, whereas the deeper phosphorus sites are kinetically protected from reacting with O_2 by slow diffusion. This demonstrates the effective oxygen-getting character of the phosphane–ene film, illustrating its utility as a flexible electronic packaging film to prevent oxygen from accessing protected sublayers.

QCM measurements were used to monitor the overall uptake of oxygen in a 48 nm MLD phosphane–ene film. Dry air (10 0.1 s pulses with 5 min purges) was delivered to a freshly prepared polymer film deposited on an Al_2O_3 -coated QCM crystal. Changes in areal mass density were monitored to determine the overall oxidation of the P sites. The QCM data show an initial sharp pressure spikes coincident with the dry air pulses, with increasing residual mass following each pulse (Figure 7b; a selected pulse is shown in the inset). After three pulses of dry air, a cumulative mass gain of 63 ng/cm^2 was

achieved. Negligible mass change was observed during subsequent dry air pulses, suggesting that the oxygen load of the phosphane–ene film had been reached. Additionally, this mass change persisted following the end of the experiment, indicating limited to no oxygen desorption. Due to the temperature-dependent nature of QCM measurements, thermal desorption could not be accurately investigated. This mass change equates to an uptake of 24 O atoms/nm². Assuming a 1:1 P/O uptake in the film, this equates to a penetration depth of oxygen of 12 nm. Repeated experiments showed limited changes to O_2 uptake, indicating low batch-to-batch variability.

CONCLUSIONS

Phosphane–ene polymer network synthesis was effectively adapted from a solution-based method to gas-phase MLD. In the proposed mechanism of film growth, the plasma-enhanced MLD process leveraged phosphinyl radical chemistry to add these species to C=C groups on a siloxane crosslinking agent (D_4^{Vinyl}) with GPCs of 0.6–2.0 Å and film thicknesses of 20–120 nm. XPS analysis highlighted bonding arrangements of P^{III} and P^V sites, demonstrating the uptake of oxygen during incidental atmospheric exposure. To assess the O_2 scavenging ability of the film, a sputtered XPS depth profile was collected. A shift from P^V to P^{III} with increasing depth was observed, which indicated surface reactivity that slows the diffusion of dioxygen through the film. Dioxygen uptake experiments by QCM characterization of unexposed, freshly prepared films showed a self-limiting mass gain of 63 ng/cm^2 equating to a penetration depth of 12 nm by oxygen of the polymer film. The high phosphorus loading and tunability of the phosphane–ene film demonstrate the promise as an oxygen scavenging packaging material, and the ability to deposit the film in a low-temperature MLD process is compatible with flexible electronics manufacturing.

EXPERIMENTAL SECTION

MLD Methods. All depositions were performed on a PICOSUN R-200 Advanced Plasma-Enhanced ALD tool. The substrates were mechanical-grade silicon (100) or Al_2O_3 -coated silicon (100). The substrates were kept in the cleanroom under ambient conditions until the wafers were diced into rectangular coupons of approximately 1 cm \times 3 cm size for use. Gold substrates were produced by coating the mechanical-grade Si wafers with approximately 100 nm of gold using a physical vapor deposition tool (Angstrom COVAP).

$i\text{BuPH}_2$ and D_4^{Vinyl} were obtained from Solvay and Sigma-Aldrich, respectively, and used as received. The D_4^{Vinyl} was observed to become viscous over time in the heated bubbler (possibly as a result of precursor oligomerization); so, for each run, the bubbler was only loaded with the amount necessary for that experiment. The $i\text{BuPH}_2$ bubbler was filled with enough material for multiple runs as it showed no sign of decomposition. Each process began with a flush step repeated three times, where high-purity (4.8 grade, 99.998%) nitrogen gas was used to fill the chamber to a pressure of 100 Torr, then evacuated to a base pressure of 5 Torr. The deposition chamber temperature was set to 200 °C and held at that temperature for 20 min prior to the precursor pulse sequence. The $i\text{BuPH}_2$ bubbler was held in a chiller at 7 °C to lower its volatility (at room temperature, a 0.1 s pulse delivered an enormous, wasteful excess of material on the order of 5 g). D_4^{Vinyl} was held at 75 °C in a “PicoSolid” bubbler, and the lines above the bubbler were held at 80 °C to prevent condensation during transit. Process nitrogen flows were set as follows: $i\text{BuPH}_2$ at 150 sccm, D_4^{Vinyl} and unused lines at 80 sccm, and intermediate space at 400 sccm. Plasma gas flows were as follows: 80 sccm carrier gas and 185 sccm plasma gas. The Ar^* pulse consisted of

a 0.4 s flow stabilization time, a 9 s plasma pulse (600 W), and no purge. The D_4^{Vinyl} pulse consisted of a 0.1–10 s pulse and a 10 s purge.

AFM Measurements. Kapton tape was placed on the substrate prior to deposition to provide a step edge of the MLD film for AFM analysis. After deposition, the tape was removed, exposing the bare Si substrate below and cleaned with isopropyl alcohol and Kimwipes. AFM analysis was performed with a Dimension 3100 SPM/AFM instrument over $\sim 50 \mu\text{m}^2$ analysis area.

XPS Measurements. Samples were transferred without an air break into a N_2 glovebox and sealed in airtight packaging to limit oxidation of the films prior to analysis. XPS analyses were carried out at Surface Science Western (SSW) with a Kratos AXIS Supra X-ray photoelectron spectrometer using a monochromatic Al K α source (15 mA, 15 kV). The sample has a depth of 7–10 nm and has detection limits ranging from 0.1 to 0.5 atomic percent. The instrument work function was calibrated to give a BE of 285 eV for the C 1s spectrum. The Kratos charge neutralizer system was used on all specimens. Both the survey scan and high-resolution analyses were collected at a take-off angle of 90° with an analysis area of $300 \times 700 \mu\text{m}$, and a pass energy of 15 eV. CasaXPS (ver. 2.3.23) software was used for all deconvolution of spectra with a Shirley background subtraction. Spectral interpretation and fittings were done with fitting parameters and constraints collected from NIST. Depth profile experiments used an Ar cluster gun with 5 keV accelerating voltage and 2000 Ar atoms.

SEM Measurements. A Leo Zeiss 1530 FIB field emission scanning electron microscope at Western's Nanofabrication facility with a magnification of 50,000 \times and an accelerating voltage of 3 kV was used. Cross sections of prepared films on SiO_2 substrates were milled out with Mo ions and observed at an angle.

QCM Measurements. All QCM measurements were conducted in a home-built hot-walled tube furnace reactor on an in situ QCM (Colnatec, EON-LT) with a built-in temperature reader. Fresh QCM crystals (6 MHz, AT-cut, Al_2O_3 electrodes) were coated and packaged as described above. The QCM was then assembled and installed into the reactor under air-free conditions. After assembly, the reactor was brought to process temperature (50°C) and left to equilibrate under no flow (0 sccm) conditions for 24 h.

After stabilizing, the polymer-coated QCM crystal was intermittently exposed to 10 pulses (100 ms) of dry air with 5 min long purges between pulses.

Adsorbed areal mass density is derived from the Sauerbrey equation²⁷

$$\frac{\Delta m}{A} = C\Delta F$$

where the conversion factor C is given by

$$C = -\frac{\sqrt{\rho\mu}}{2f_0^2}$$

where the density of a quartz crystal (ρ_q) is 2.648 g cm^{-3} , the shear modulus of an AT-cut crystal (μ_{AT}) is $2.947 \times 10^{11} \text{ g cm}^{-1} \text{ s}^{-2}$, and a resonant frequency of 6 MHz provides a conversion factor of $-12.27 \text{ ng cm}^{-2} \text{ Hz}^{-1}$.

The areal oxygen density ($\#_O/A$) is calculated using the following relationship

$$\frac{\#_O}{A} = \frac{N_A \times (\Delta m/A)}{MW_O}$$

where N_A is the Avogadro number, $\Delta m/A$ is the areal mass density, and MW_O is the molecular weight of oxygen.

Thermogravimetric Analysis. Air-free TGA was performed on a TA Instruments Discovery TGA 55 instrument housed in a nitrogen-filled (99.998%) MBraun LABmaster 130 glovebox. In a typical experiment, approximately 25 mg of analyte was placed in a platinum pan and heated to 400°C with a ramp rate of $10^\circ\text{C}/\text{min}$. Nitrogen (99.999% purity, 60 sccm) was used as the process gas. Platinum pans

were cleaned by sequential sonication in glacial acetic acid, then isopropanol, followed by heating until red-hot with a propane torch.

Differential Scanning Calorimetry. DSC experiments were performed with a TA Instruments Q10 instrument. The instrument was calibrated at the melting point of indium metal (156.6°C). All DSC samples were hermetically sealed in aluminum pans inside a glovebox prior to analysis. All samples were heated to 500°C with a ramp rate of $10^\circ\text{C}/\text{min}$, using nitrogen (99.998% purity, 50 sccm) as the process gas.

■ ASSOCIATED CONTENT

Supporting Information

The Supporting Information is available free of charge at <https://pubs.acs.org/doi/10.1021/acs.chemmater.2c03036>.

DSC, SEM, XPS, and AFM data (PDF)

■ AUTHOR INFORMATION

Corresponding Authors

Seán T. Barry – Department of Chemistry, Carleton University, Ottawa, Ontario K1S 5B6, Canada; Email: seanbarry@cunet.carleton.ca

Paul J. Ragona – Department of Chemistry, University of Western Ontario, London, Ontario N6A 3K7, Canada; orcid.org/0000-0003-2727-7635; Email: pragogna@uwo.ca

Authors

Justin T. Lomax – Department of Chemistry, University of Western Ontario, London, Ontario N6A 3K7, Canada

Eden Goodwin – Department of Chemistry, Carleton University, Ottawa, Ontario K1S 5B6, Canada

Peter G. Gordon – Department of Chemistry, Carleton University, Ottawa, Ontario K1S 5B6, Canada

Christine McGuiness – Solvay USA Inc., Alpharetta, Georgia 30005, United States

Floryan De Campo – Solvay USA Inc., Alpharetta, Georgia 30005, United States

Complete contact information is available at:

<https://pubs.acs.org/10.1021/acs.chemmater.2c03036>

Author Contributions

The manuscript was written through contributions of all authors. All authors have given approval to the final version of the manuscript.

Funding

Solvay Canada, Natural Science and Engineering Research Council of Canada (NSERC) and Ontario Ministry of Research and Innovation (OMRI).

Notes

The authors declare no competing financial interest.

■ ACKNOWLEDGMENTS

The authors would like to thank the Natural Sciences and Engineering Council of Canada (NSERC), the Canada Foundation for Innovation (CFI), Solvay Specialty Polymers, Surface Science Western (SSW; Drs. M. Biesinger and J. Henderson), the Western Nanofabrication Facility, Carleton Nanofab, Western University and Carleton University for their support.

■ REFERENCES

(1) Meng, X. An Overview of Molecular Layer Deposition for Organic and Organic–Inorganic Hybrid Materials: Mechanisms,

- Growth Characteristics, and Promising Applications. *J. Mater. Chem. A* **2017**, *5*, 18326–18378.
- (2) Yoshimura, T.; Tatsura, S.; Sotoyama, W. Polymer Films Formed with Monolayer Growth Steps by Molecular Layer Deposition. *Appl. Phys. Lett.* **1991**, *59*, 482–484.
- (3) Kim, A.; Filler, M. A.; Kim, S.; Bent, S. F. Layer-by-Layer Growth on Ge(100) via Spontaneous Urea Coupling Reactions. *J. Am. Chem. Soc.* **2005**, *127*, 6123–6132.
- (4) Yoshimura, T.; Tatsura, S.; Sotoyama, W.; Matsuura, A.; Hayano, T. Quantum Wire and Dot Formation by Chemical Vapor Deposition and Molecular Layer Deposition of One-dimensional Conjugated Polymer. *Appl. Phys. Lett.* **1992**, *60*, 268–270.
- (5) Ivanova, T. V.; Maydannik, P. S.; Cameron, D. C. Molecular Layer Deposition of Polyethylene Terephthalate Thin Films. *J. Vac. Sci. Technol. A* **2012**, *30*, 01A121.
- (6) Loscutoff, P. W.; Lee, H.-B.-R.; Bent, S. F. Deposition of Ultrathin Polythiourea Films by Molecular Layer Deposition. *Chem. Mater.* **2010**, *22*, 5563–5569.
- (7) Guterman, R.; Rabiee Kenaree, A.; Gilroy, J. B.; Gillies, E. R.; Ragogna, P. J. Polymer Network Formation Using the Phosphane–Ene Reaction: A Thiol–Ene Analogue with Diverse Postpolymerization Chemistry. *Chem. Mater.* **2015**, *27*, 1412–1419.
- (8) Béland, V. A.; Ragogna, P. J. Metallized Phosphane–Ene Polymer Networks as Precursors for Ceramics with Excellent Shape Retention. *ACS Appl. Mater. Interfaces* **2020**, *12*, 27640–27650.
- (9) Cuthbert, T. J.; Guterman, R.; Gillies, E. R.; Blacquire, J.; Gilroy, J.; Ragogna, P. J. Polymerization of Primary Phosphines with Olefins to Generate Phosphorus Based Polymer Networks. U.S. Patent US 20,200,270,399 A1, 2020.
- (10) Béland, V. A.; Wang, Z.; Sham, T.-K.; Ragogna, P. J. Antimony-Functionalized Phosphine-Based Photopolymer Networks. *Angew. Chem., Int. Ed.* **2018**, *57*, 13252–13256.
- (11) Béland, V. A.; Ragogna, P. J. Metallized Phosphane–Ene Polymer Networks as Precursors for Ceramics with Excellent Shape Retention. *ACS Appl. Mater. Interfaces* **2020**, *12*, 27640–27650.
- (12) Stiles, A. R.; Rust, F. F.; Vaughan, W. E. The Preparation of Organo-Phosphines by the Addition of Phosphine to Unsaturated Compounds. *J. Am. Chem. Soc.* **1952**, *74*, 3282–3284.
- (13) Béland, V. A.; Wang, Z.; Sham, T.-K.; Ragogna, P. J. Polymer Networks Functionalized with Low-Valent Phosphorus Cations. *J. Polym. Sci.* **2022**, *60*, 2508–2517.
- (14) Salin, I. M.; Seferis, J. C. Kinetic Analysis of High-Resolution TGA Variable Heating Rate Data. *J. Appl. Polym. Sci.* **1993**, *47*, 847–856.
- (15) Price, D. M. Vapor Pressure Determination by Thermogravimetry. *Thermochim. Acta* **2001**, *367–368*, 253–262.
- (16) Kunte, G. V.; Ail, U.; Ajikumar, P. K.; Tyagi, A. K.; Shivashankar, S. A.; Umarji, A. M. Estimation of Vapour Pressure and Partial Pressure of Subliming Compounds by Low-Pressure Thermogravimetry. *Bull. Mater. Sci.* **2011**, *34*, 1633–1637.
- (17) Price, D. M. A Fit of the Vapours. *Thermochim. Acta* **2015**, *622*, 44–50.
- (18) Lin, S.-Y.; Tsai, T.-K.; Lin, C.-M.; Chen, C.; Chan, Y.-C.; Chen, H.-W. Structures of Self-Assembled Monolayers of *n*-Alkanoic Acids on Gold Surfaces Modified by Underpotential Deposition of Silver and Copper: Odd–Even Effect. *Langmuir* **2002**, *18*, 5473–5478.
- (19) Barranco, V.; Carpentier, J.; Grundmeier, G. Correlation of Morphology and Barrier Properties of Thin Microwave Plasma Polymer Films on Metal Substrate. *Electrochim. Acta* **2004**, *49*, 1999–2013.
- (20) Coclite, A. M.; Howden, R. M.; Borrelli, D. C.; Petruczok, C. D.; Yang, R.; Yagüe, J. L.; Ugur, A.; Chen, N.; Lee, S.; Jo, W. J.; Liu, A.; Wang, X.; Gleason, K. K. 25th Anniversary Article: CVD Polymers: A New Paradigm for Surface Modification and Device Fabrication. *Adv. Mater.* **2013**, *25*, 5392–5423.
- (21) Jones, R. G.; Ando, W.; Chojnowski, J. *Silicon-Containing Polymers: The Science and Technology of Their Synthesis and Applications*; Springer Science & Business Media, 2013.

(22) Ashurbekova, K.; Ashurbekova, K.; Saric, I.; Gobbi, M.; Modin, E.; Chuvilin, A.; Petravic, M.; Abdulagatov, I.; Knez, M. Ultrathin Hybrid Si/AlCOH Dielectric Films through Ring-Opening Molecular Layer Deposition of Cyclic Tetrasiloxane. *Chem. Mater.* **2021**, *33*, 1022–1030.

(23) O'Hare, L.-A.; Parbhoo, B.; Leadley, S. R. Development of a Methodology for XPS Curve-Fitting of the Si 2p Core Level of Siloxane Materials. *Surf. Interface Anal.* **2004**, *36*, 1427–1434.

(24) O'Hare, L.-A.; Hynes, A.; Alexander, M. R. A Methodology for Curve-Fitting of the XPS Si 2p Core Level from Thin Siloxane Coatings. *Surf. Interface Anal.* **2007**, *39*, 926–936.

(25) Barr, T. L.; Seal, S. Nature of the Use of Adventitious Carbon as a Binding Energy Standard. *J. Vac. Sci. Technol. A* **1995**, *13*, 1239–1246.

(26) Swift, P. Adventitious Carbon—the Panacea for Energy Referencing? *Surf. Interface Anal.* **1982**, *4*, 47–51.

(27) Johannsmann, D. *The Quartz Crystal Microbalance in Soft Matter Research; Soft and Biological Matter*; Springer International Publishing: Cham, 2015.

Recommended by ACS

Additive Manufacturing by Heating at a Patterned Photothermal Interface

Chang-Uk Lee, Andrew J. Boydston, *et al.*

MARCH 20, 2023

ACS APPLIED MATERIALS & INTERFACES

READ 

Stabilization of Dinuclear Rhodium and Iridium Clusters on Layered Titanate and Niobate Supports

Ritesh Uppuluri, Thomas E. Mallouk, *et al.*

NOVEMBER 09, 2022

INORGANIC CHEMISTRY

READ 

Trapping an Unusual Ring-Opened Product of THF within a Lithium Hydrido Aluminate

Matthew J. Evans, Martyn P. Coles, *et al.*

SEPTEMBER 26, 2022

ORGANOMETALLICS

READ 

Further Proof of Unconventional Conjugation via Disiloxane Bonds: Double Decker Sesquioxane [vinylMeSi(O_{0.5})₂(PhSiO_{1.5})₈(O_{0.5})₂SiMeviny] Derived ...

Zijing Zhang, Richard M. Laine, *et al.*

SEPTEMBER 13, 2022

MACROMOLECULES

READ 

Get More Suggestions >